Programmed assembly of bespoke prototissues on a microfluidic platform

Kaitlyn Ramsay, Jae Levy, Pierangelo Gobbo & Katherine S. Elvira

2021

Programmed assembly of bespoke prototissues on a microfluidic platform

Kaitlyn Ramsay,[1,2] Jae Levy,[1] Pierangelo Gobbo[3,*] and Katherine S. Elvira[1,2,*]

[1]Department of Chemistry, University of Victoria, Victoria, Canada

[2]The Centre for Advanced Materials and Related Technology (CAMTEC), University of Victoria, Victoria, Canada

[3]School of Chemistry, University of Bristol, Bristol, United Kingdom

[*]kelvira@uvic.ca

Abstract

The precise assembly of protocell building blocks into prototissues that are stable in water, capable of sensing the external environment and which display collective behaviours remains a considerable challenge in prototissue engineering. We have designed a microfluidic platform that enables us to build bespoke prototissues from predetermined compositions of two types of protein-polymer protocells. We can accurately control their size, composition and create unique Janus configurations that are not possible with traditional methods. Because we can control the number and type of the protocells that compose the prototissue, we can hence modulate the collective behaviours of this biomaterial. We show control over both the amplitude of thermally induced contractions in the biomaterial and its collective endogenous biochemical reactivity. Our results show that microfluidic technologies enable a new route to the precise and high-throughput fabrication of tissue-like materials with programmable collective properties that can be tuned through careful assembly of protocell building blocks of different types. We anticipate that our bespoke prototissues will be a starting point for the development of more sophisticated artificial tissues for use in medicine, soft robotics, and environmentally beneficial bioreactor technologies.

Introduction

This past decade has shown a surge of work in the field of bottom-up synthetic biology. Most seeks to address the gap between biology and chemistry in order to better understand how self-assembled non-living molecular systems become life. To do this, attempts have been made to construct "non-typical protocells".[1] These are non-living, artificial cell-like entities created from scratch using only a limited toolbox of molecules, materials, and chemical reactions and aim to mimic basic features of living cells.[1–3] Conversely, "typical protocells" are designed to mimic key behaviours of living cells.[4] To date, researchers have engineered a range of different non-typical protocells using many different types of materials to build the artificial cell membrane, giving rise to protocells made from lipid bilayers,[5,6] polymers,[7–9] polypeptides,[10] dendrimers,[11] inorganic nanoparticles[12,13] and coacervate microdroplets.[14–16] Each type of material used to build the protocell membrane enables different features of biological cells to be modelled. Proteinosomes are an emerging non-typical protocell model, which are generated as Pickering emulsions from amphiphilic protein-polymer nanoparticles, termed nanoconjugates. Proteinosomes have a semi-permeable and elastic membrane which consists of a closely packed single layer of protein-polymer nanoparticles in the form of bovine serum albumin/poly(N-isopropylacrylamide (BSA/PNIPAM) amphiphilic nanoconjugates. The BSA/PNIPAM membrane is then chemically crosslinked with PEG-bis(N-succinimidyl succinate) (PEG-diNHS) so that the proteinosomes can be transferred from a water/oil biphasic system into a solely water media for applications in synthetic biology. The advantages of proteinosomes as a protocell model include the permeability of the membrane and their ability to respond to changes in temperature.[10] Moreover, proteinosomes have been engineered to display cell-like behaviours such as selective permeability,[10,17] gene-directed protein synthesis,[18] internalised enzyme catalysis,[19,20] predatory behaviours[21] and reversible contractility.[22]

There has been increasing interest in devising methods to assemble protocell units into tissue-like materials called "prototissues" that mimic basic aspects of biological tissues such as chemical communication, contractility and enzyme mediated metabolism. One such example used magnetic fields to manipulate diamagnetic giant unilamellar lipid vesicles (GUVs) into coded configurations.[23] Another example used micro-arrays of hemi-fused GUVs which could be patterned *via* acoustic standing waves. A 3D printing technique to pattern water-in-oil droplets connected *via* interface bilayers (DIBs) into synthetic tissues showed that DIBs were capable of membrane protein mediated electrical communication, deformation and light-induced gene expression.[24] While these different approaches have provided important breakthroughs in prototissue design and construction, they are not without their drawbacks. The diamagnetic GUVs require aqueous media containing high levels of toxic $MnCl_2$ and a constant magnetic field to maintain the patterns. Additionally, they are not stable in *in vivo* conditions and, as such, are not indicative of true life-like structures. When using standing waves, these need to be constantly

applied to avoid a rapid re-dispersal of the GUVs into the bulk solution. Lastly, the 3D-printing of DIBs requires the presence of an external bulk oil phase, and they have a short shelf-life.

In contrast, Gobbo and co-workers recently developed a synthetic approach to the programmed assembly of small prototissue spheroids based on the interfacial covalent adhesion of two populations of chemically reactive protocells.[25] They developed proteinosome membranes functionalised with either azide or bicyclononyne (BCN) functional groups and used Pickering emulsification to assemble them into spheroids with a of ~75–200 μm as water-in-oil-in-water (w/o/w) multicompartmental droplets. Removal of the inner oil phase by dialysis then triggered an interfacial strain-promoted alkyne-azide cycloaddition (I-SPAAC) reaction between the two different types of proteinosomes, resulting in robust spheroidal clusters of covalently linked protocells. They then showed that these prototissue spheroids were capable of reversible contractions, which could be enzymatically modulated and exploited for mechanochemical transduction. However, the bulk emulsification method used was based on the manual shaking of a vial and did not allow control over the number of protocells that composed the prototissue nor their spatial organisation. This severely limited our ability to further investigate and modulate the interesting collective properties of the biomaterial.

Here we have designed a microfluidic platform that enables the programmed assembly of chemically reactive protocells into prototissues of bespoke size and composition. Microfluidic tools have been largely used for the bottom-up synthesis of non-typical protocells,[26–28] including proteinosomes.[29] However, the development microfluidic methods for the bottom-up assembly of artificial tissues from artificial cells is still in its infancy. This is in contrast to the use of microfluidic technologies for the creation of living tissues from living cells (organs-on-a-chip), which is a thriving field with applications in medicine and drug discovery.[30–34] In this work we report the first example of a microfluidic platform for the simultaneous fabrication of two proteinosome populations functionalised with either azide or BCN-functional groups at high throughput and with narrow size distribution, and their assembly into prototissues with high control over their composition and 3D architecture. Our microfluidic platform allowed us to systematically vary the number of each type of protocell from 1 to 10 as well as their ratio within each prototissue. This was instrumental in allowing us to elucidate new behaviours of the biomaterial. For example, we were able to show the key role of the covalent protocell-protocell adhesions formed through the SPAAC reaction in the mechanism of the thermally induced collective contractility of the prototissues and fine tune the amplitude of the reversible contractions. We also show that by controlling the number and type of the protocells that compose the prototissues, it was possible to modulate the collective endogenous biochemical reactivity of the overall tissue-like material. Our results show that microfluidic techniques provide otherwise unattainable opportunities and insight into prototissue engineering. Our microfluidic platform opens a route to the fabrication of robust prototissues, whose emergent bio-inspired capabilities can be carefully programmed and modulated by precisely assembling protocell building blocks of different type.

Results and Discussion

A microfluidic platform for the creation of bespoke prototissues

Our microfluidic platform for the formation of bespoke prototissues was fabricated from polydimethylsiloxane (PDMS) using conventional soft lithography techniques. To create the prototissues, w/o/w multiple emulsions were formed using specific variations of previous microfluidic designs that enabled the formation of these multiple emulsions from droplets stabilised by biological molecules.[35–37] Our platform consisted of three flow focusing junctions (Figure 1a), two of which are placed in parallel and used for the formation of the proteinosomes (our protocell model), which were water-in-oil (w/o) Pickering emulsion droplets stabilised by either rhodamine B isothiocyanate (RITC)-labelled azide-functionalised BSA/PNIPAM-co-MAA nanoconjugates (RITC-labelled protocells, red fluorescence) or fluorescein isothiocyanate-labelled BCN-functionalised BSA/PNIPAM-co-MAA nanoconjugates (FITC-labelled protocells, green fluorescence) and chemically crosslinked with a PEG-diNHS crosslinker. Each of these flow focusing junctions was composed of a 50 μm wide inlet channel which fed a solution of protein-polymer nanoconjugate (8 mg mL^{-1}) and PEG-diNHS (160 mg mL^{-1}) in Na_2CO_3 buffer (100 mM, pH 8.5) to the junction, two 50 μm wide carrier phase channels through which the oil phase flowed, and a 100 μm wide exit channel with a pinched entrance section that was 25 μm wide (Figure 1a).

A third flow focusing junction was placed in series and used for the encapsulation of pre-determined numbers of FITC- and RITC-labelled protocells to form w/o/w droplets stabilised as a Pickering emulsion by an unlabelled BSA/PNIPAM-co-MAA outer membrane. As shown in our prior work, once the oil is removed, this outer membrane tightly enveloped (cages) the RITC- and FITC-labelled protocells to form the prototissues. This flow focusing junction was composed of a 200 μm wide inlet channel (from the combination of the two 100 μm wide channels carrying the w/o droplets), two 200 μm wide channels for the aqueous carrier phase (a solution of non-reactive unlabelled BSA/PNIPAM-co-MAA nanoconjugate at a concentration of 8 mg mL^{-1}), and a 400 μm wide exit channel with a pinched 200 μm wide entrance (Figure 1a). The large width of the exit channel allowed for

the encapsulation of up to 10 RITC- and FITC-labelled protocells within one outer membrane. In contrast to the first two flow focusing junctions, in this flow focusing junction the inlet channel (which carries the protocells) and the carrier phase channels (which carry the oil phase) were specifically designed to be perpendicular to each other to generate high enough shear forces for the creation of the w/o/w droplets.

In all three flow focusing junctions, an increase in the diameter of the exit channels was required to slow down the flow rate. Moreover, the region between the two sets of flow focusing junctions had to be long enough to allow the stabilisation of the RITC- and FITC-labelled protocells. At all flow focusing junctions, the combination of the slower flow rate and the shear forces created by the pinching flows of the carrier phases allowed for the formation of single w/o or multiple w/o/w droplets stabilised by different types of BSA/PNIPAM-co-MAA nanoconjugates. The final notable feature of the microfluidic platform was a meander, which was used to image the w/o/w droplets. Surface treatment of the microfluidic channels was key for the generation of stable proteinosome-based protocells and prototissues. The section of the microfluidic platform used for the creation of protocells was kept hydrophobic, whereas the section of the platform used for the creation of prototissues was made hydrophilic through surface treatment with polyvinyl alcohol (PVA, 0.01 mg mL^{-1}). Additionally, it was important to prime the hydrophilic channels with the unlabelled BSA/PNIPAM-co-MAA nanoconjugate solution prior to inserting the oil phase to stabilise the formation of prototissues. The FITC- and RITC-labelled protocells produced at the two first flow focusing junctions had a very narrow size distribution and a diameter of 45.07 ± 1.89 μm and 45.66 ± 1.90 μm, respectively (Figure S1). Comparison of these results with those obtained for proteinosomes produced using a bulk methodology showed a significant decrease of the relative standard deviation of the size distributions from 72.7% and 69.5% to 4.2% and 4.2%, respectively. These results compare well with data reported from a microfluidic platform used to fabricate one type of non-reactive proteinosomes from a BSA/PNIPAM nanoconjugate (27.1 ± 1.0 μm in diameter, relative standard deviation 3.7%).[29]

The design of the third flow focusing junction allowed us to create w/o/w droplets that encapsulated a pre-determined number of FITC- or/and RITC-labelled protocells that could be varied from 1 to 10 (Videos S1-S7). Sizes could easily be tailored by changing flow rate ratios but to showcase the ability of our microfluidic platform to generate prototissue spheroids with controlled size, composition, and configuration the ratios in this work remained constant. This level of control was achieved by systematically decreasing the flow rate of the outer aqueous phase. For example, a mono-compartmental w/o/w droplet containing a single RITC- or FITC-labelled protocell could be formed by setting the flow rate of the outer aqueous phase to 330 μL min^{-1}, the flow rate of the oil phase to 6 μL min^{-1}, and the flow rates of the two inner aqueous phases to 1 μL min^{-1} each. Multicompartment w/o/w droplets with increasing numbers of RITC- or FITC-labelled protocells could be generated by sequentially decreasing the flow rate of the outer aqueous phase by 20 μL min^{-1} and keeping the flow rates of the oil phase and of the inner aqueous phases the same (6 μL min^{-1} and 1 μL min^{-1} each, respectively). Figure 1b shows brightfield (left) and fluorescence microscopy images (right) of six different w/o/w droplets generated using this methodology. The number of enclosed protocells was systematically varied from 1 to 2, 4, 6, 8 and 10, and the protocell fraction of the multicompartment w/o/w droplets, defined as the ratio between enclosed RITC-labelled protocells and the total number of enclosed protocells, was kept at 0.5. We called these droplets mono-, 1a,1b bi-, 2a,2b tetra-, 3a,3b hexa-, 4a,4b octa-, and 5a,5b deca-compartmental w/o/w droplets, respectively. As similarly described in the work of Farley and coworkers,[38] the nomenclature is as follows: the number of RITC-labelled protocells ("a", red) and FITC-labelled protocell ("b", green) is specified at the beginning of the name. This is followed by the suffix (bi-, tri-, tetra-, penta-, etc.), which indicates the total number of protocells enclosed in each w/o/w droplet. The precision and accuracy (target number) with which we could enclose the desired number of protocells was found to progressively decrease with the increasing target number of enclosed protocells (Figure 1c). For example, while an individual FITC- or RITC-labelled protocell could be enclosed within the outer membrane with 100% accuracy and precision, a 1:1 binary population of 5 RITC- and 5 FITC-labelled protocells could be enclosed with only 10% success. This follows the trend shown in prior work for more complex multiple emulsion systems.[38] However, since the microfluidic platform could produce between 5 and 15 w/o/w droplets per second, we were able to generate between 9,000 and 27,000 deca-compartmental w/o/w droplets in only 30 minutes (Video S8).

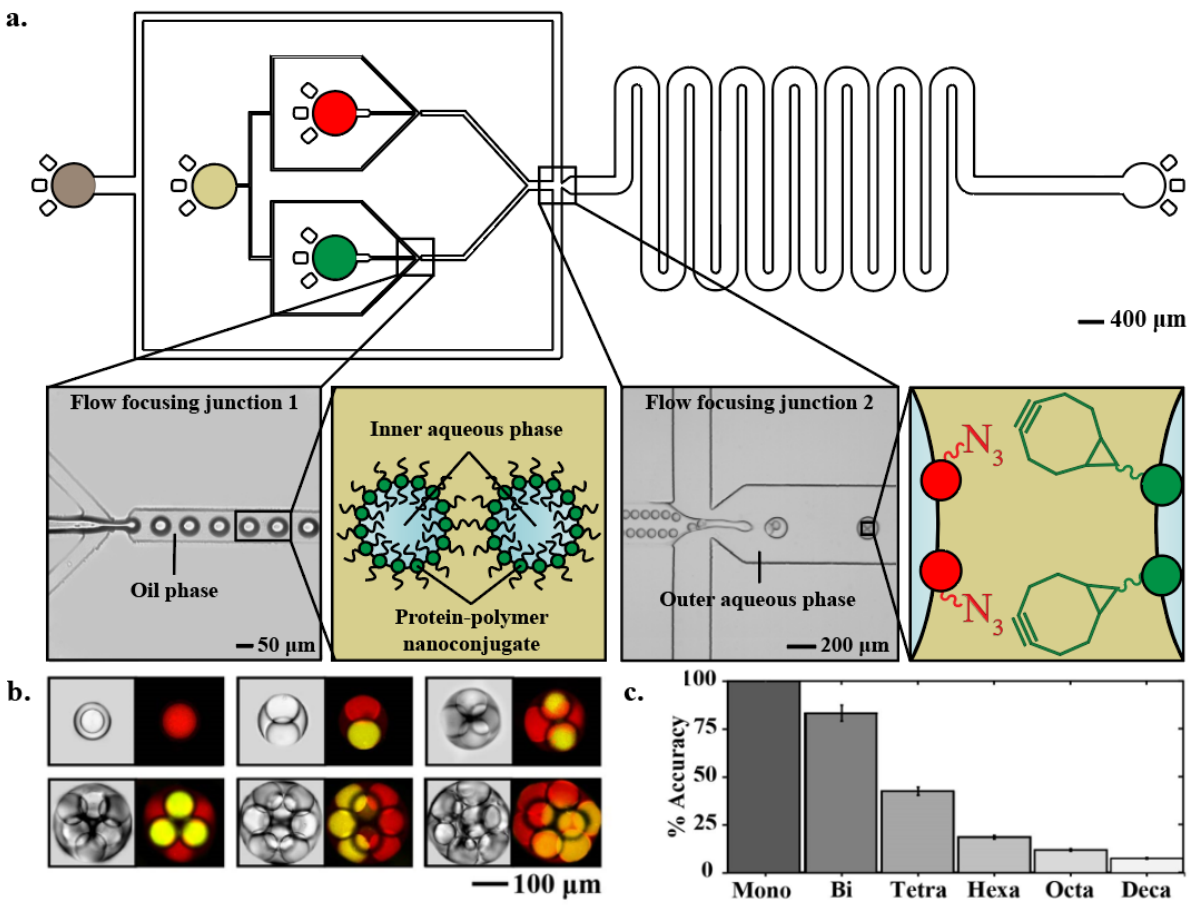

Figure 1. Microfluidic generation of prototissues. a) Scheme showing the design of our microfluidic platform. The inner phases of the two parallel flow focusing junctions at the centre of the device were comprised of either an aqueous solution of RITC-labelled azide-functionalised BSA/PNIPAM-co-MAA nanoconjugate and PEG-diNHS to make RITC-labelled protocells (inlet highlighted with a red circle, top) or an aqueous solution of FITC-labelled BCN-functionalised BSA/PNIPAM-co-MAA nanoconjugate and PEG-diNHS to make FITC-labelled protocells (inlet highlighted with a green circle, bottom). The oil phase (inlet highlighted with a yellow circle) was 2-ethyl-1-hexanol. The outer aqueous phase of the third flow focusing junction (inlet highlighted with a brown circle, left) was comprised of a solution of unlabelled non-reactive BSA/PNIPAM-co-MAA nanoconjugate that creates the outer membrane of the prototissue. Droplet formation at both types of flow focusing junctions is shown with insets containing microscopy images of the droplets on the microfluidic device and a scheme explaining the composition of the droplets. These schemes show the stabilisation of the aqueous protocell droplets, and the type of functional groups present on the surface of the two types of protocells. The cycloaddition reaction between the azide (represented by red N_3 groups) and BCN (represented by green 8-membered rings) moieties to form covalent bonds between the two types of protocells occurs off-chip due to the removal of the oil phase that separates the droplets. This allows the formation of the prototissues. At the first two flow focusing junctions (left), protocells were formed as w/o droplets with BSA nanoconjugates self-assembled at the water-oil interface. At the third flow focusing junction (right) a 1a,1b bi-compartmental emulsion was formed from one FITC-labelled protocell and one RITC-labelled protocell. **b)** Brightfield (left) and fluorescent (right) microscopy images of mono- and multicompartmental w/o/w droplets. From top left to bottom right: w/o/w droplet containing a single RITC-labelled protocells (red fluorescence), bi-, tetra-, hexa-, octa- and deca-compartmental w/o/w droplets with equal numbers of RITC-labelled protocells (red fluorescence) and FITC-labelled protocells (green fluorescence). **c)** Graph showing the analysis of the device performance for the generation of targeted multicompartment w/o/w droplets. For each type of droplet, data was acquired on three different microfluidic devices. In each case, a total of 90 w/o/w droplets were analysed. All measurements were performed using ImageJ. Error bars represent the standard deviation.

The microfluidic platform allowed us to spatially divide the protocells within the prototissues, resulting in multicompartment w/o/w droplets with a Janus configuration (Figure 1b). This was achieved by designing the third flow focusing junction such that the two inlet streams containing each type of protocell joined together in a single inlet channel without mixing, with the RITC-labelled protocells lined up in the top half of the channel and the FITC-labelled protocells lined up in the bottom half of the channel. Video S9 shows how the protocells enclosed within the outer membrane of the droplet moved according to well-known flow recirculation effects.[39] Due to the symmetry of the inner droplet flux (the flow of the inner droplets relative to the outer), they did not mix, and this resulted in the maintenance of the predetermined Janus-like organisation. However, by addition of

a meander prior to the third flow focusing junction it is also possible to create non-Janus prototissues. Being able to generate Janus multicompartment droplets by spatially assembling protocell building blocks with high precision is an important achievement in bottom-up synthetic biology. This allows us to break up the symmetry of the prototissues, opening a route, for example, towards the generation of endogenous gradients of chemical signals.

Our microfluidic platform not only enabled us to control the total number of protocells that composed the prototissues, but it also allowed us to create multicompartment systems of tailored composition with any predetermined protocell ratio. This could be achieved by changing the ratio between the flow rates of the two inner aqueous phases. For example, if the desired ratio was 3 RITC-labelled protocells and 1 FITC-labelled protocell, then the flow rate of the RITC-labelled inner phase needed to be 3 times greater than that of the FITC-labelled inner aqueous phase. Hence, to fabricate, for example, 3a,1b tetra-compartmental w/o/w droplets, the flow rate of the inner aqueous phase containing the RITC-labelled azide-functionalised BSA/PNIPAM-co-MAA nanoconjugate was set to 0.75 μL min^{-1}, whereas the flow rate of the inner aqueous phase containing the FITC-labelled BCN-functionalised BSA/PNIPAM-co-MAA nanoconjugate was set to 0.25 μL min^{-1}. Figure 2 shows a library of all possible combinations of w/o/w droplets with a total number of protocells between 1 to 10 that could be generated using our microfluidic platform. All combinations showed the preferential Janus-like configuration of the protocell building blocks. This figure shows representative images from highly reproducible data (data were reproduced on three different microfluidic devices). Due to the control offered by our microfluidic platform, the three-dimensional (3D) packing of the protocells can be controlled and predicted. As all protocells are generated *in situ* with a narrow size distribution (Figure S1), the space between them can be assumed to be a three-dimensional Euclidean space. As a result, the equally sized spheres represented by our protocells self-organise in a lattice. As the total number of protocells in the prototissue increases, we can clearly observe how the protocells form a symmetric, close-packed structure and preferentially form a face-centred cubic lattice. Since our microfluidic platform enables us to form protocells of equal size, we can make prototissues that are densely packed and have predictable structures as shown in Figure 1b and Figure 2.

Significantly, in all cases, removal of the encapsulated oil phase *via* dialysis off-chip enabled the chemically reactive RITC-labelled azide- and FITC-labelled BCN-functionalised protocells enclosed within the non-reactive outer membrane to form covalent adhesion points *via* the I-SPAAC reaction as reported previously,[25] and produce membrane-bound prototissues that were stable in water. These results show, for the first time, that microfluidic technologies can be used to assemble bespoke prototissues from protein-polymer artificial cells at high throughput and with precise sizes and compositions; enabling new possibilities in prototissue engineering.

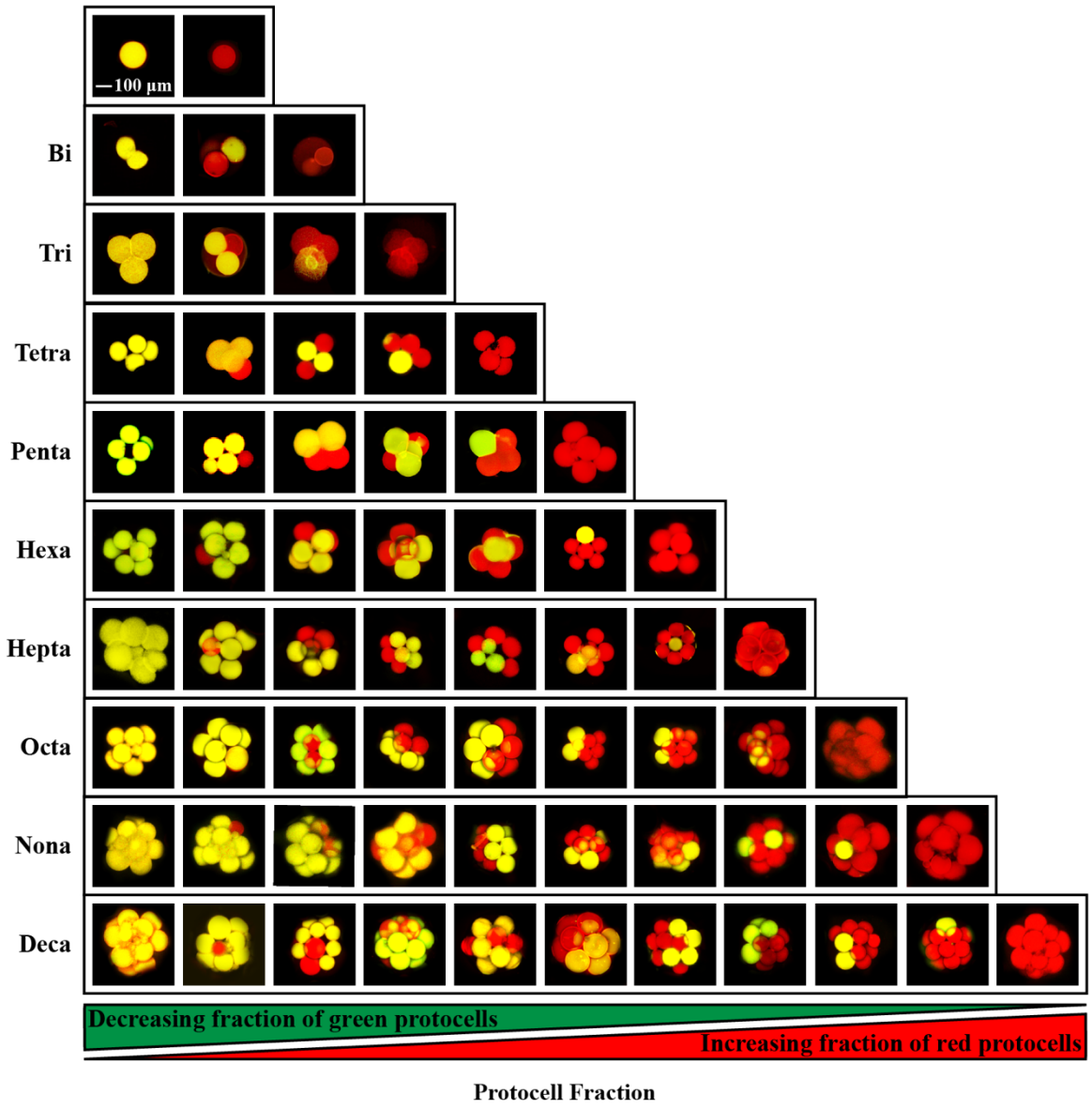

Figure 2. Preferred geometric configurations of bespoke multicompartment w/o/w droplets. Representative fluorescence confocal microscopy images showing single FITC- and RITC-labelled protocells (top) to deca-compartmental w/o/w droplets (bottom) made from all possible combinations of RITC-labelled protocells (red fluorescence) and FITC-labelled protocells (green fluorescence). On the left-hand side of each row, the w/o/w droplets have the maximum number of FITC-labelled protocells (protocell fraction = 0). Each subsequent image has a progressively increasing number of RITC-labelled protocells. On the right-hand side of each row, w/o/w droplets have the maximum number of RITC-labelled protocells (protocell fraction = 1). Data was reproduced on at least three different microfluidic devices. The scale bar (top left) applies to all images.

Influence of the composition of the prototissues on thermally induced reversible contractions

Having established that our microfluidic platform allowed us to readily assemble bespoke prototissues with predetermined protocell fractions and with specific 3D architectures, next we studied the changes in the amplitude of the thermally induced contractions of the prototissues as a function of protocell composition. The BSA/PNIPAM-co-MAA nanoconjugates that form the membrane of our proteinosome protocells contain a thermoresponsive polymer (PNIPAM-co-MAA). Hence, this assay was designed to study the collective thermoresponsive behaviour of our biomaterial. To achieve this, we fabricated 21 different samples of bi- to deca-compartmental w/o/w droplets and systematically changed their composition by changing the protocell fraction on-chip. Subsequently, the corresponding prototissues were assembled by forming protocell-protocell adhesions *via* the I-SPAAC reaction by removing the inner oil phase through dialysis off-chip. All samples were then heated to 47 °C, *i.e.* above the lower critical solution temperature (LCST) of PNIPAM-co-MAA which is around 36 °C (Figure S2), and the temperature-dependent changes in the equilibrium size of all prototissues were analysed by fluorescence confocal microscopy. This contraction is reversible.[25] Figure 3a (and Figure S3) summarise our

findings and show that, in general, the amplitude of the thermally induced volume contractions progressively increases from bi- to deca-prototissues. For each type of prototissue, when the protocell fraction was either 0 (only FITC-labelled protocells) or 1 (only RITC-labelled protocells) the prototissues displayed the smallest volume contractions, whereas the volume contractions progressively increased when the protocell fraction approached 0.5, that is when the number of RITC- and FITC-labelled protocells was the same. In fact, for the bi-, tetra-, and deca-compartmental prototissues assembled with a protocell fraction of 0.5, we observed the highest volume contractions. More specifically, the amplitude of the contractions went from 12 ± 10 vol% for the 0a,2b (or 2a,0b) bi-compartmental prototissues to 42 ± 7 vol% for the 1a,1b bi-compartmental prototissues (an increase of *ca.* 336%); from 29 ± 5 vol% for the 0a,4b (or 4a,0b) tetra-compartmental prototissues to 51 ± 5 vol% for the 2a,2b tetra-compartmental prototissues (an increase of *ca.* 179%); and from 42 ± 5 vol% for the 1a,9b (or 9a,1b) deca-compartmental prototissues to 57 ± 3 vol% for the 5a,5b deca-compartmental prototissues (an increase of *ca.* 136%). In contrast, individual FITC or RITC-labelled protocells caged within an outer unlabelled BSA/PNIPMA-co-MAA membrane contracted only up to 5 ± 2 vol%. The reversible contractions of protocells and prototissues take place when the temperature rises above the LCST of PNIPAM-co-MAA. Above the LCST the polymer chains undergo a conformational change from coil to globule while expelling water molecules. This macromolecular mechanical contraction happens on the crosslinked protein-polymer nanoconjugates that compose a protocell membrane, causing a slight contraction (5 ± 2 vol%) of the entire micro-compartment. Our results highlight how the contraction of an individual protocell is however amplified when a high number of protocell units are covalently linked together, indicating an emerging collective contractile behaviour of our covalently linked prototissues.

To further investigate the enhanced volume contractions of the prototissues assembled at a protocell fraction of 0.5, we used the microfluidic platform to fabricate 3a,3b hexa- and 4a,4b octa-compartmental prototissues. The samples were then heated to 47 °C, and the temperature-dependent changes in the equilibrium size of the prototissues were analysed by fluorescence confocal microscopy. Figure 3b summarises our results and shows that the amplitude of the contractions rapidly increased from individual protocells enclosed within a non-reactive BSA/PNIPAM-co-MAA outer membrane to 1a,1b bi-compartmental prototissues. However, the amplitude of the contractions across the series reached a threshold limit of *ca.* 60 vol% despite the increasing number of protocells at a protocell fraction of 0.5. We attribute this to the Janus configuration of the prototissues, which limits the contact area between the FITC- and RITC-labelled protocell building blocks, especially for larger prototissues. For images of the prototissues at both their starting (26 °C) and ending (47 °C) temperatures refer to Figure S4. These observations are consistent with previously reported results for prototissues of random composition fabricated using bulk methodologies[25] and clearly indicate that the amplitudes of the collective thermoresponsive contractions of the prototissues are proportional to the number of covalent adhesions between FITC- and RITC-labelled protocells The larger the contact area between the FITC- and RITC-labelled protocells that compose the prototissue, the more enhanced the volume contraction. We attribute this to increased interactions between the PNIPAM-co-MAA chains of covalently linked proteinosome protocell membranes, which make the expulsion of water molecules from the material at temperatures above the LCST more effective, with a consequent enhanced contraction of the overall proteinosome assembly. From a more general perspective, for the first time our microfluidic platform has allowed us to systematically assemble prototissues with increasing numbers of proteinosome protocells as well as vary the protocell fraction to control the amplitude of the thermally induced collective contractions. Most importantly, this allowed us to provide important experimental results in support of our initial hypothesis that the covalent protocell-protocell adhesions formed through the I-SPAAC reaction are primarily responsible for the collective thermoresponsive contractility of the prototissues.[25]

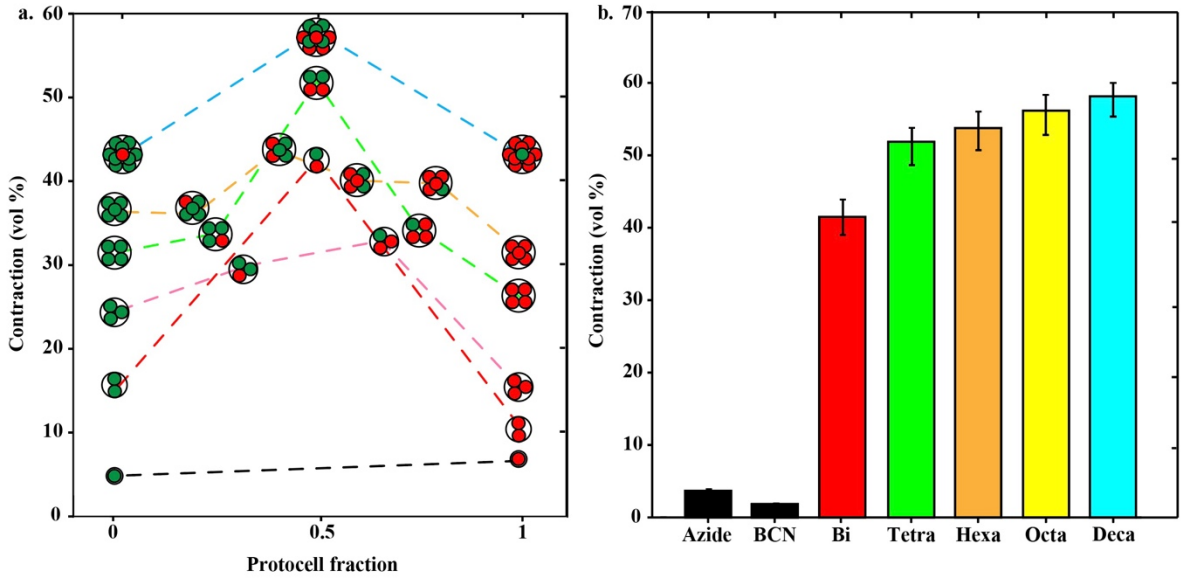

Figure 3. Collective thermoresponsive reversible contractile behaviour of bespoke prototissue. a) Graph showing the percent volume contraction of prototissues of different composition when the temperature is varied from 26 °C to 47 °C. The x-axis shows the protocell fraction, defined as the ratio between the number of RITC-labelled protocells and the total number of protocells in the prototissue. For clarity, each datapoint is represented with a cartoon representing the composition of the prototissue that was measured. Raw data and error analysis are reported in Figure S3. **b)** Graph showing the percent volume contraction for 1a,1b bi-, 2a,2b tetra-, 3a,3b hexa-, 4a,4b octa-, 5a,5b deca-compartmental prototissues when the temperature is varied from 26 °C to 47 °C. The "Azide" label refers to a single RITC-labelled azide-functionalised protocell enclosed within a non-reactive BSA/PNIPAM-co-MAA outer membrane. The "BCN" label refers instead to a single FITC-labelled BCN-functionalised protocell enclosed within a non-reactive BSA/PNIPAM-co-MAA outer membrane. Values are the average of measurements from 3 different prototissues. Error bars represent the standard deviation.

Modulation of the endogenous biochemical reactivity of the prototissues

Then we explored the possibility of exploiting the high control over the prototissue composition provided by our microfluidic platform to regulate the endogenous biochemical reactivity of the prototissues. To achieve this, we prepared deca-compartmental prototissues comprising 5 unlabelled azide-functionalised protocells and 5 FITC-labelled protocells that were pre-loaded with GOx or horseradish peroxidase (HRP), respectively. The azide-functionalised protocells were not labelled with RITC during these experiments to ensure that we could detect the red-fluorescent product of the enzyme reaction. We then added the prototissues to an aqueous solution containing the proteinosome-permeable molecular substrates glucose (14 mM) and Amplex Red (0.5 mM) to initiate an internalised and spatially coupled GOx/HRP enzyme cascade reaction. In this reaction, glucose and Amplex Red freely diffused through the system and were transformed into gluconic acid and resorufin, respectively (Figure 4a). We used UV-Vis spectroscopy to monitor the onset of endogenous production of the red resorufin product caused by the completion of the enzyme cascade so that we could analyse multiple prototissues simultaneously. Figure 4b shows that the onset of red absorbance took place immediately with an initial velocity $v_0 = 200$ μM s^{-1}, and reached maximum absorbance after around 30 min. In contrast, control experiments carried out by removing either glucose or Amplex Red showed no increase in absorbance due to the inability of the prototissues to produce the signalling molecule H_2O_2 or to produce a fluorescent output signal, respectively (Figures S5-S7). Next, we used our microfluidic platform to create two additional samples of different deca-compartmental prototissues. The first sample contained prototissues made from 1 HRP-containing unlabelled azide-functionalised protocell and 9 GOx-containing FITC-labelled protocells, also called an enzymatically active 1a,9b deca-prototissue. The second sample contained prototissues made from 9 HRP-containing unlabelled protocells and 1 GOx-containing FITC-labelled protocell (enzymatically active 9a,1b deca-prototissues). Both samples were perfused in an aqueous solution of glucose and Amplex Red to initiate the same spatially coupled internalised GOx/HRP enzyme cascade reaction described above. However, this time, due to the different protocellular composition, the initial velocities of the two samples were much lower. The enzymatically active 9a,1b, deca-compartmental prototissue sample had a v_0 of 30 μM s^{-1}, whereas the enzymatically active 1a,9b deca-compartmental prototissue sample had a v_0 of 100 μM s^{-1} (Figure 4b, S5 and S7). These results show that our microfluidic platform allows us to effectively regulate the endogenous catalytic reactivity of prototissues by controlling the number and type of protocells.

The marked difference in the initial rate of the enzyme cascade rection between the 5a(GOx),5b(HRP)-deca-compartmental prototissues and the other two samples was attributed to an overall high and equal number of protocells of both kinds (i.e., GOx- and HRP-containing protocells) that compose the material. The reason for the highest initial rate displayed by the 1a(GOx),9b(HRP)-deca-compartmental prototissues compared to the 9a(GOx),1b(HRP)-deca-compartmental prototissue was instead attributed to the rate limiting step of the enzyme cascade reaction being the production of resorufin.[40] This indicates that controlling the number and type of protocells that compose of prototissue not only allows us to fine-tune the biochemical reactivity of the material, but also to identify specific rate limiting steps of their endogenous bioactivity.

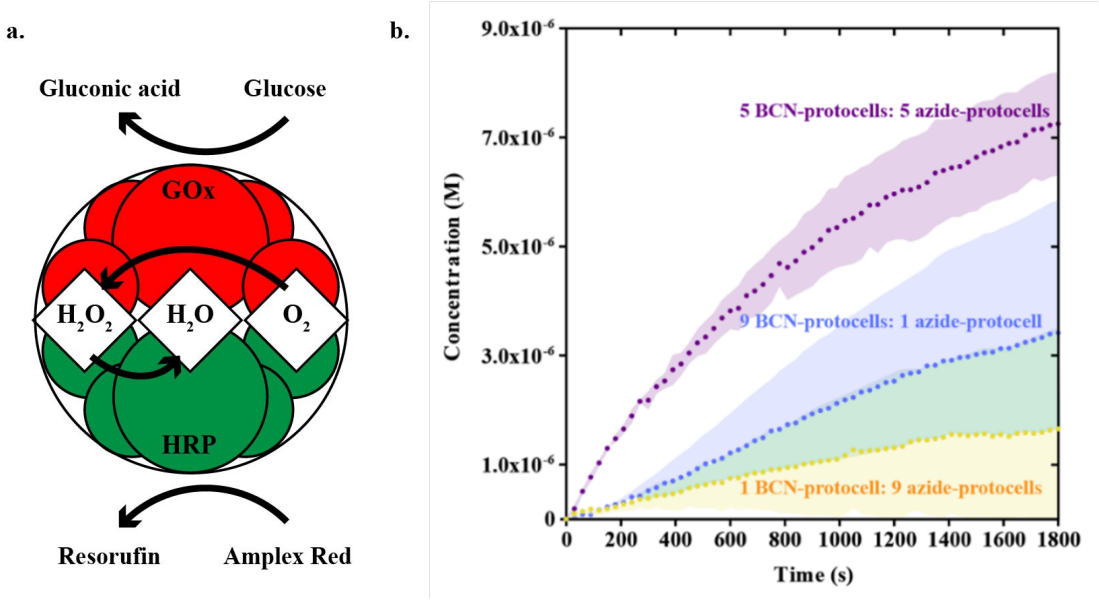

Figure 4. Modulation of the endogenous biochemical reactivity of the prototissues. a) Scheme showing the GOx/HRP enzyme cascade reaction in a 5a,5b deca-compartmental prototissue consisting of 5 HRP-containing unlabelled azide-functionalized protocells (red circles) and 5 GOx-containing FITC-labelled protocells (green circles). The substrates glucose and Amplex Red freely diffuse through the membranes of the prototissue. The GOx-containing protocells oxidise glucose to gluconic acid and H_2O_2. This initiates radial diffusion of H_2O_2 from the GOx-containing protocells, which is then used by the HRP-containing protocells to oxidise the non-fluorescent molecules Amplex Red to red fluorescent resorufin. H_2O_2 can therefore be considered as a signalling molecule between the two interlinked protocell communities. **b)** Graph showing time-dependent changes in the concentration of the final resorufin product for the enzyme cascade described in **a**) for a sample of 5a,5b deca-compartmental prototissues consisting of 5 HRP-containing unlabelled azide-functionalized protocells and 5 GOx-containing FITC-labelled protocells (purple plot), a sample of 1a,9b deca-compartmental prototissues consisting of 1 HRP-containing unlabelled azide-functionalized protocells and 9 GOx-containing FITC-labelled protocells (blue plot), and a sample of 9a,1b deca-compartmental prototissues consisting of 9 HRP-containing unlabelled azide-functionalized protocells and 1 GOx-containing FITC-labelled protocell (yellow plot). Data were acquired by UV-Vis spectroscopy by measuring the time-dependent changes in absorbance at 560 nm. Experiments were reproduced in triplicate. Kinetics reach steady state over the course of the experiment (data now shown). Statistical variation in the data is shown as coloured bands which represent the standard deviation of the data.

Conclusions

In conclusion, we have engineered a microfluidic platform that, for the first time, allows the simultaneous creation of two proteinosome-based protocell populations at high throughput and with narrow size distribution, and their assembly into prototissues with high control over their composition. Notably, the assembled prototissues displayed a Janus architecture, which was obtained by lining up the two different types of protocells within the microfluidic device. Being able to generate Janus prototissues through spatial assembly of individual protocell building blocks with high precision is an important achievement in bottom-up synthetic biology. The possibility of segregating different protocell types within a prototissue architecture will open up a route to the engineering of tissue-like materials capable of chemotactic behaviours,[41,42] and to the generation of endogenous gradients of chemical signals, which could be exploited for the investigation of the physicochemical basis of important biological processes such as embryogenesis, wound healing, and cancer metastasis.

The high control over the assembly of the prototissues enabled by our microfluidic platform also allowed us to elucidate the key role of the covalent protocell-protocell adhesions in the mechanism of the thermally induced collective contractility of the prototissues and fine tune the amplitude of the contractions. Similarly, we were able to show that the endogenous biochemical reactivity of prototissues could be modulated by controlling the number

and types of the protocells that compose them. These results open up a new methodology for the fabrication of artificial tissue-like materials with programmable emergent biochemical activities that can be regulated through careful assembly of protocell building blocks of different types using a microfluidic platform. Overall, our results show that microfluidic technologies provide invaluable opportunities in prototissue engineering, allowing for the precise assembly of different protocell types into prototissues with programmable and tuneable collective capabilities. From a more general perspective, the possibility of fine tuning the collective properties of prototissues by controlling their composition enables potential applications of this new bespoke biomimetic material in biotechnology, soft robotics and environmentally beneficial bioreactor technologies.

Materials and Methods

Materials

All reagents were used as received. Trichloromethysilane, 2-ethyl-1-hexanol, sodium bicarbonate, glucose oxidase (GOx) from Aspergillus niger (10000 U), beta-glucose, hydrolysed polyvinyl alcohol (PVA, 87-90%), O,O'-bis[2-(N-succinimidyl-succinylamino)ethyl]polyethylene glycol (PEG-diNHS) and dialysis bags (MWCO 12–14 kDa) were purchased from Millipore Sigma. Amplex Red Hydrogen Peroxide/Peroxidase Assay Kit was purchased from ThermoFisher Scientific. Acetate masks were printed at 10 μm resolution by CAD/Art Services. SU-8 3050 and developer were purchased from MicroChem. Silicon wafers (100 mm diameter) were purchased from Silicon Materials. Polydimethylsiloxane (PDMS, Dow Sylgard 184) was purchased from Ellsworth Adhesives. Polytetrafluoroethylene (PTFE) tubing (1/16" outer diameter, 750 μm inner diameter) was purchased from Chromatographic Specialties. Jensen global 20 gauge IT series blunt stainless steel needles were purchased from Howard Electronics.

Synthesis of starting materials

RITC-labelled azide-functionalised, FITC-labelled BCN-functionalised, and unlabelled non-reactive BSA/PNIPAM-co-MAA nanoconjugates were synthesised as described in detail in the supporting information of our previously published work.[25] This required multiple steps, first by synthesising PNIPAM-co-MAA and labelling BSA with fluorescent dyes. We then synthesised cationised BSA and conjugated this to the thermoresponsive polymer to form the BSA/PNIPAM-co-MAA nanoconjugate. This nanoconjugate was then functionalised with either azide- or BCN to give both to create the molecules that form the membrane of both types of protocells used in this work.

Fabrication of microfluidic devices

Microfluidic platforms were designed using AutoCAD (Autodesk Student 2017 LTD) and printed onto acetate masks to create positive photomasks. The SU-8 layer was spin-coated onto the wafer at a thickness of 50 ± 2 μm as determined using a DektakXT Stylus Profiler. Next, the wafer was soft baked for 5 min at 25 °C, 2 min at 65 °C and 30 min at 95 °C. Following the soft bake, the wafer was exposed to UV light for 11 s at 19.96 mW cm^{-2} using an OAI Model 800 mask aligner through the acetate photomask. The wafer was then heated at 95 °C for 15 min and cooled for 30 min. Unexposed SU-8 was removed using developer and the adhesion of the features was enhanced through exposure to UV light for 90 s at 19.96 mW cm^{-2} and a final hard bake for 30 min at 200°C. The wafer was then placed in a glass desiccator with 50 μL of trimethylchlorosilane and put under vacuum for 1 h to deposit a thin film of silane onto the surface of the wafer. A 10:1 ratio of PDMS base to curing agent was added to a 3D printed wafer holder which was designed to hold the wafer and a set volume of PDMS. The PDMS was degassed for 1 h under vacuum and then cured overnight at 65 °C. The cured PDMS was peeled from the mould and individual devices were cut out using a scalpel. The inlets and outlets were created using a 1 mm biopsy punch. The channels were sealed with PDMS-coated glass microscope slides. These slides were made by spin coating PDMS (prepared as described above) onto the slides at 1200 rpm for 25 s. Both the PDMS-coated glass slides and the PDMS devices were washed prior to bonding in soapy reverse osmosis water, reverse osmosis water, isopropyl alcohol, ethanol, Milli-Q water, and then blown dry with filtered air and baked at 95 °C for 30 min.

Surface treatment of microfluidic devices

This surface treatment protocol is modified from prior work.[43] The PVA solution was made by adding PVA to MilliQ water at a final concentration of 0.01 mg mL^{-1}. The solution was stirred at room temperature at 1200 rpm for 45 min, at 100 °C at 1200 rpm for 45 min and then at 65 °C at 1200 rpm overnight. The solution was used within 24 h. Prior to surface treatment, the PDMS devices and PDMS-coated slides were treated with air plasma (Diener Electronic, Zepto ONE, 1 min, 100 W, 0.64 mbar) to activate the surfaces, and the slide and device were then placed into contact with each other to covalently bond their surfaces. The microfluidic devices were allowed to sit for approximately 2 min. Next, a 25 mL syringe filled with air was fitted with a 20 G syringe tip that had

been heat-ligated to 25 cm of PTFE tubing. The syringe was placed into an Aladdin Single-Syringe Infusion Pump (World Precision Instruments) which was set to 800 μL min^{-1}. Next, a 1 mL glass gas-tight syringe (Hamilton) was filled with the PVA solution and connected to tubing as described above. The two innermost inlets on the platform (green and red circles, Figure 1a), were plugged with heat-sealed PTFE tubing, the aqueous inlet (brown circle) was connected to a 12 cm length of PTFE tubing to act as an outlet during surface treatment, the middle inlet (yellow circle) was connected to the PTFE tubing connected to the air-filled syringe and the platform outlet (white) was attached to the syringe filled with PVA solution. The pump was turned on and allowed to pump for a minimum of 1 min. After this, the PVA solution was pushed manually into the platform until the liquid reached the third flow focusing junction, at which point the interface was held steady for 10 min. Then, the inlet attached to the air-filled syringe was removed and attached to a filtered air gun so that the PVA solution could be blown out of the device. The surface treated microfluidic device was then placed on a hot plate for 15 min at 110 °C, and stored at 65 °C for a minimum of 72 h prior to use.

Generation of multicompartmental prototissues using the microfluidic platform and measurement of their thermally induced reversible contractions

First, a solution of PEG-diNHS crosslinker 160 mg mL^{-1} in Na_2CO_3 buffer (100 mM, pH 8.5) was made. For the inner aqueous phase, 1 mL solutions comprising 500 μL of PEG-diNHS solution and 500 μL of the desired azide- or BCN-functionalised protein-polymer nanoconjugate solution were prepared and inserted into the inner inlets of the platform using 1 mL glass gas-tight syringes (Figure 1a, green and red circles). The oil phase consisted of 2-ethyl-1 hexanol (Figure 1a, yellow circle). The outer phase solution was made by dissolving 250 μL of unlabelled non-reactive BSA/PNIPAM-co-MAA nanoconjugate solution (8 mg mL^{-1}) in 25 mL of 1 M Na_2CO_3. A 25 mL glass gas-tight syringe was used to insert the outer aqueous phase into the microfluidic platform. In order to connect all glass syringes to the microfluidic devices, 5 equal lengths (approximately 25 cm) of PTFE tubing were cut and heat ligated to 20 G syringe tips. The syringes were then placed into 4 neMESYS 290N low pressure syringe pumps (Cetoni) and the tips of the tubing were inserted into the respective inlets and outlets. A Phantom VEO710L high-resolution, high-speed camera was used for imaging. The flow rates were set as follows: outer phase to 250 μL min^{-1}, middle phase to 6 μL min^{-1}, and both inner phases to 1 μL min^{-1}. All pumps were started at the same time and were allowed to equilibrate within the platform for approximately 2 min whereby the first multiple emulsions would begin to form. This allows the outer phase to prime the channels prior to droplet formation and equilibration in a similar manner to priming the surfaces of channels with oil as is done commonly in the field. Once this occurred, the outermost flow rate could be tuned to either increase or decrease the encapsulation ratio of the droplets. After collection, the excess outer phase solution was removed using a micropipette. Then, 500 μL of a solution of PEG-diNHS crosslinker in water (160 mg mL^{-1}) were added to the prototissue sample in an approximately 1:1 ratio and the mixture was left in the dark at room temperature for 72 h. After this, the oil was removed *via* dialysis with 70% ethanol in MilliQ water for 3-4 h, followed by 30% ethanol in MilliQ water for 3-4 h, and finally MilliQ water for 18 h. This is the standard procedure for the formation of prototissues.[25] Prototissues were introduced into a chamber created on microscope slide, which was placed onto a temperature stage (LTS420, Likham) on a LSM 880 Zeiss confocal laser scanning microscope. Excitation was provided by either a 488 nm Argon laser (FITC) or 561 nm laser (RITC). For thermoresponsivity experiments, the temperature was varied between 26 °C and 47 °C and 2 min were allowed for equilibration at each temperature. The changes in the prototissue cross-sectional area were determined using ImageJ (version 1.47t). All data were acquired in triplicate, where each repetition was from a completely new prototissue sample. All images were taken at either 20x or 50x wide-angle magnification.

Bulk generation of FITC- and RITC-labelled proteinosome as w/o droplets

In a 1.75 mL glass vial, 30 μL of an aqueous solution of RITC-labelled azide- or FITC-labelled BCN-functionalised BSA/PNIPAAm-co-MAA nanoconjugates (8 mg mL^{-1}) and 30 μL of a solution PEG-diNHS (67 mg mL^{-1}) in Na_2CO_3 buffer (pH 8.5, 100 mM) were mixed together. Subsequently, 1 mL of 2-ethyl-1-hexanol was gently added to the aqueous phase. Due to the hydrophilic nature of the azide- and BCN-functionalised BSA/PNIPAM-co-MAA nanoconjugates, a polar oil is needed to generate stable Pickering emulsions under the conditions reported. This is because the amphiphilic nanoparticles (protein-polymer nanoconjugates) self-assemble at the water oil interface. The mixture was shaken manually for 30 s to produce a white turbid solution. The changes in the proteinosome cross-sectional area were determined using ImageJ (version 1.47t).

Horseradish peroxidase (HRP)/glucose oxidase (GOx) enzyme cascades

Multicompartmental prototissues comprised of different ratios of HRP-containing unlabelled azide-functionalised proteinosomes and GOx-containing FITC-labelled BCN-functionalised proteinosomes (5a,5b deca-prototissues, 1a,9b deca-prototissues, and 9a,1b deca-prototissues) were created on the microfluidic platform using the same procedure described above. In order to enclose the enzyme inside the desired proteinosomes, an aqueous solution of the enzyme was co-dissolved with the appropriate protein-polymer nanoconjugate for use as the inner aqueous

phase in the microfluidic device. To generate the HRP-containing unlabelled azide-functionalised proteinosomes, 12 μL of a solution of HRP (1000 U mL^{-1}) were added to a 1 mL solution of PEG-diNHS and unlabelled azide-functionalised BSA/PNIPAM-co-MAA nanoconjugate. To generate the GOx-containing FITC-labelled BCN-functionalised proteinosomes, 12 μL of a solution of GOx (1000 U mL^{-1}) were added to the 1 mL solution of PEG-diNHS and FITC-labelled BCN-functionalised BSA/PNIPAM-co-MAA nanoconjugate. After the generation of the desired enzymatically active w/o/w multicompartmental droplets, the corresponding prototissues were generated using dialysis following the procedure outlined above. UV-Vis spectroscopy (SpectraMax M5) was used for the visualisation of the biochemical reactivity of the prototissues. To 125 μL of a dispersion of prototissues was added 37.5 μL of a solution of glucose (300 mM) in MilliQ water and 1.25 μL of a solution of Amplex Red (150 mM) in MilliQ water. The enzyme-mediated generation of the red fluorescent final product resorufin was followed by monitoring the absorbance at 560 nm. Automated path length correction was activated to correct for volume differences between the wells, and a reading was recorded every 30 s. Control experiments were performed in the same way but either the glucose or Amplex Red solution was substituted with the same volume of MilliQ water.

Acknowledgements

This research was funded through Dr Elvira's Natural Sciences and Engineering Research Council of Canada (NSERC) Discovery grant. Dr Elvira's position is funded through the Canada Research Chair program and the Michael Smith Foundation for Health Research Scholar in partnership with the Pacific Alzheimer Research Foundation. Her laboratory was equipped using funding from the Canada Foundation for Innovation John R. Evans Leaders Fund, the British Columbia Knowledge Development Fund (BCKDF) and the NSERC Research Tools and Instruments program. The authors thank the Centre for Advanced Materials and Related Technology (CAMTEC) at the University of Victoria for access to confocal microscopy and cleanroom facilities, and Dr Stanislav Konorov for help with confocal microscopy. Dr Gobbo was supported by a University of Bristol Vice-Chancellor's Fellowship and an EPSRC New Investigator Award (Grant Ref: EP/T01508X/1).

Author Contributions

KSE, PG and KR conceived the experiments, performed data analysis and discussed the results. KR performed the experimental work. JL assisted with the enzyme experiments. KSE and KR designed and developed the microfluidic platform. KSE supervised KR and JL. PG synthesised and characterised the protein-polymer nanoconjugates. All authors contributed to drafts of the manuscript. KSE, PG and KR wrote the final manuscript.

References

1 C. Xu, S. Hu and X. Chen, Artificial cells: from basic science to applications, *Materials Today*, 2016, **19**, 516–532.
2 N. A. Yewdall, A. F. Mason and J. C. M. van Hest, The hallmarks of living systems: towards creating artificial cells, *Interface Focus*, 2018, **8**, 20180023.
3 A. Pohorille and D. Deamer, Artificial cells: prospects for biotechnology, *Trends in Biotechnology*, 2002, **20**, 123–128.
4 P. Gobbo, From protocells to prototissues: a materials chemistry approach, *Biochemical Society Transactions*, 2020, **48**, 2579–2589.
5 K. Kurihara, Y. Okura, M. Matsuo, T. Toyota, K. Suzuki and T. Sugawara, A recursive vesicle-based model protocell with a primitive model cell cycle, *Nature Communications*, 2015, **6**, 8352.
6 N. P. Kamat, S. Tobé, I. T. Hill and J. W. Szostak, Electrostatic Localization of RNA to Protocell Membranes by Cationic Hydrophobic Peptides, *Angewandte Chemie International Edition*, 2015, **54**, 11735–11739.
7 A. F. Mason and P. Thordarson, Polymersomes as protocellular constructs, *Journal of Polymer Science Part A: Polymer Chemistry*, 2017, **55**, 3817–3825.
8 A. Kubilis, A. Abdulkarim, A. M. Eissa and N. R. Cameron, Giant Polymersome Protocells Dock with Virus Particle Mimics via Multivalent Glycan-Lectin Interactions, *Scientific Reports*, 2016, **6**, 32414.
9 W.-S. Jang, S. C. Park, E. H. Reed, K. P. Dooley, S. F. Wheeler, D. Lee and D. A. Hammer, Enzymatically triggered rupture of polymersomes, *Soft Matter*, 2016, **12**, 1014–1020.
10 X. Huang, M. Li, D. C. Green, D. S. Williams, A. J. Patil and S. Mann, Interfacial assembly of protein–polymer nano-conjugates into stimulus-responsive biomimetic protocells, *Nature Communications*, 2013, **4**, 2239.
11 P. Torre, Q. Xiao, I. Buzzacchera, S. E. Sherman, K. Rahimi, N. Yu. Kostina, C. Rodriguez-Emmenegger, M. Möller, C. J. Wilson, M. L. Klein, M. C. Good and V. Percec, Encapsulation of hydrophobic components in dendrimersomes and decoration of their surface with proteins and nucleic acids, *Proceedings of the National Academy of Sciences*, 2019, **116**, 15378 LP – 15385.

12 J.-P. Douliez, N. Martin, T. Beneyton, J.-C. Eloi, J.-P. Chapel, L. Navailles, J.-C. Baret, S. Mann and L. Béven, Preparation of Swellable Hydrogel-Containing Colloidosomes from Aqueous Two-Phase Pickering Emulsion Droplets, *Angewandte Chemie International Edition*, 2018, **57**, 7780–7784.
13 A. San Miguel and S. H. Behrens, Permeability control in stimulus-responsive colloidosomes, *Soft Matter*, 2011, **7**, 1948–1956.
14 N. Martin, M. Li and S. Mann, Selective Uptake and Refolding of Globular Proteins in Coacervate Microdroplets, *Langmuir*, 2016, **32**, 5881–5889.
15 J. Fothergill, M. Li, S. A. Davis, J. A. Cunningham and S. Mann, Nanoparticle-Based Membrane Assembly and Silicification in Coacervate Microdroplets as a Route to Complex Colloidosomes, *Langmuir*, 2014, **30**, 14591–14596.
16 A. Mason, L. Abdelmohsen, N. A. Yewdall, B. Buddingh, D. Williams and J. Van Hest, in *Abstracts of Papers of the American Chemical Society*, 2018.
17 X. Huang, A. J. Patil, M. Li and S. Mann, Design and Construction of Higher-Order Structure and Function in Proteinosome-Based Protocells, *Journal of the American Chemical Society*, 2014, **136**, 9225–9234.
18 P. L. Luisi, M. Allegretti, T. Pereira de Souza, F. Steiniger, A. Fahr and P. Stano, Spontaneous Protein Crowding in Liposomes: A New Vista for the Origin of Cellular Metabolism, *ChemBioChem*, 2010, **11**, 1989–1992.
19 Y. Yin, H. Chang, H. Jing, Z. Zhang, D. Yan, S. Mann and D. Liang, Electric field-induced circulation and vacuolization regulate enzyme reactions in coacervate-based protocells, *Soft Matter*, 2018, **14**, 6514–6520.
20 B. V. V. S. P. Kumar, A. J. Patil and S. Mann, Enzyme-powered motility in buoyant organoclay/DNA protocells, *Nature Chemistry*, 2018, **10**, 1154–1163.
21 C. Zhao, M. Zhu, Y. Fang, X. Liu, L. Wang, D. Chen and X. Huang, Engineering proteinosomes with renewable predatory behaviour towards living organisms, *Materials Horizons*, 2020, **7**, 157–163.
22 T. Wang, J. Xu, X. Fan, X. Yan, D. Yao, R. Li, S. Liu, X. Li and J. Liu, Giant "Breathing" Proteinosomes with Jellyfish-like Property, *ACS Applied Materials & Interfaces*, 2019, **11**, 47619–47624.
23 Q. Li, S. Li, X. Zhang, W. Xu and X. Han, Programmed magnetic manipulation of vesicles into spatially coded prototissue architectures arrays, *Nature Communications*, 2020, **11**, 232.
24 A. Alcinesio, O. J. Meacock, R. G. Allan, C. Monico, V. Restrepo Schild, I. Cazimoglu, M. T. Cornall, R. Krishna Kumar and H. Bayley, Controlled packing and single-droplet resolution of 3D-printed functional synthetic tissues, *Nature Communications*, 2020, **11**, 2105.
25 P. Gobbo, A. J. Patil, M. Li, R. Harniman, W. H. Briscoe and S. Mann, Programmed assembly of synthetic protocells into thermoresponsive prototissues, *Nature Materials*, 2018, **17**, 1145–1153.
26 M. Ugrinic, A. deMello and T.-Y. D. Tang, Microfluidic Tools for Bottom-Up Synthetic Cellularity, *Chem*, 2019, **5**, 1727–1742.
27 O. Staufer, M. Schröter, I. Platzman and J. P. Spatz, Bottom-Up Assembly of Functional Intracellular Synthetic Organelles by Droplet-Based Microfluidics, *Small*, 2020, **16**, 1906424.
28 F. Lussier, O. Staufer, I. Platzman and J. P. Spatz, Can Bottom-Up Synthetic Biology Generate Advanced Drug-Delivery Systems?, *Trends in Biotechnology*, , DOI:https://doi.org/10.1016/j.tibtech.2020.08.002.
29 M. Ugrinic, A. Zambrano, S. Berger, S. Mann, T.-Y. D. Tang and A. deMello, Microfluidic formation of proteinosomes, *Chemical Communications*, 2018, **54**, 287–290.
30 S. N. Bhatia and D. E. Ingber, Microfluidic organs-on-chips, *Nat Biotechnol*, 2014, **32**, 760–772.
31 D. E. Ingber, Reverse Engineering Human Pathophysiology with Organs-on-Chips, *Cell*, 2016, **164**, 1105–1109.
32 M. Rothbauer, J. M. Rosser, H. Zirath and P. Ertl, Tomorrow today: organ-on-a-chip advances towards clinically relevant pharmaceutical and medical in vitro models, *Current Opinion in Biotechnology*, 2019, **55**, 81–86.
33 M. Mastrangeli and J. van den Eijnden-van Raaij, Organs-on-chip: The way forward, *Stem Cell Reports*, 2021, **16**, 2037–2043.
34 K. S. Elvira, Microfluidic technologies for drug discovery and development: friend or foe?, *Trends in Pharmacological Sciences*, 2021, **42**, 518–526.
35 G. T. Vladisavljević, R. Al Nuumani and S. A. Nabavi, Microfluidic Production of Multiple Emulsions, *Micromachines (Basel)*, , DOI:10.3390/mi8030075.
36 W. Wang, R. Xie, X.-J. Ju, T. Luo, L. Liu, D. A. Weitz and L.-Y. Chu, Controllable microfluidic production of multicomponent multiple emulsions, *Lab Chip*, 2011, **11**, 1587–1592.
37 W. Wang, M.-J. Zhang and L.-Y. Chu, Microfluidic approach for encapsulation via double emulsions, *Current Opinion in Pharmacology*, 2014, **18**, 35–41.
38 S. Farley, K. Ramsay and K. S. Elvira, A plug-and-play modular microcapillary platform for the generation of multicompartmental double emulsions using glass or fluorocarbon capillaries, *Lab Chip*, , DOI:10.1039/D1LC00126D.

39 H. Song, J. D. Tice and R. F. Ismagilov, A Microfluidic System for Controlling Reaction Networks in Time, *Angewandte Chemie International Edition*, 2003, **42**, 768–772.
40 C. N. Baroud, F. Gallaire and R. Dangla, Dynamics of microfluidic droplets, *Lab Chip*, 2010, **10**, 2032.
41 A. Joseph, C. Contini, D. Cecchin, S. Nyberg, L. Ruiz-Perez, J. Gaitzsch, G. Fullstone, X. Tian, J. Azizi, J. Preston, G. Volpe and G. Battaglia, Chemotactic synthetic vesicles: Design and applications in blood-brain barrier crossing, *Science Advances*, 2017, **3**, e1700362.
42 I. A. B. Pijpers, S. Cao, A. Llopis-Lorente, J. Zhu, S. Song, R. R. M. Joosten, F. Meng, H. Friedrich, D. S. Williams, S. Sánchez, J. C. M. van Hest and L. K. E. A. Abdelmohsen, Hybrid Biodegradable Nanomotors through Compartmentalized Synthesis, *Nano Letters*, 2020, **20**, 4472–4480.
43 T. Trantidou, Y. Elani, E. Parsons and O. Ces, Hydrophilic surface modification of PDMS for droplet microfluidics using a simple, quick, and robust method via PVA deposition, *Microsystems & Nanoengineering*, 2017, **3**, 16091.